International Journal of Machine Tools and Manufacture 123 (2017) 48–56

Contents lists available at ScienceDirect

International Journal of Machine Tools and Manufacture

journal homepage: www.elsevier.com/locate/ijmactool

A multiscale evaluation of the surface integrity in boring trepanning association deep hole drilling

Huang Zhang [a,1], Xingquan Shen [a,*], Arixin Bo [b,1], Yaoming Li [a], Haifei Zhan [b,c], Yuantong Gu [b,**]

[a] School of Mechanical Engineering, North University of China, Taiyuan, 030051, China
[b] School of Chemistry, Physics and Mechanical Engineering, Queensland University of Technology (QUT), Brisbane, QLD 4001, Australia
[c] School of Computing, Engineering and Mathematics, Western Sydney University, Penrith, NSW 2751, Australia

ARTICLE INFO

Keywords:
BTA deep hole drilling
Surface integrity
Deformation
Hardness
Machining parameters

ABSTRACT

Boring trepanning association (BTA) deep hole drilling is one of the most important manufacturing techniques to produce a large length-to-diameter ratio hole for industrial applications. In addressing the challenge of excessive surface damage, inefficiency and poor indexing in BTA deep hole drilling, for which there are limited studies reported. The functional behaviour of deep hole machining and the correlation between the machined surface quality, subsurface layer deformation and the machining conditions are investigated in this paper, together with the drilling mechanism. Various parameter combinations are used to produce different samples on which surface roughness and microstructures are studied. Metallurgical characterization is performed on the subsurface regions, followed by qualitative and quantitative mechanical nanohardness investigations. Electron microscopic analysis reveals various surface features such as grooves and plateaus, folding, material flaking that are exclusive to deep hole drilling. It has been found that improved surface integrity in BTA drilling relies on a trade-off among feedrates and speeds. Although considered sample dependent, combination of a feedrate of 28 mm min^{-1} and a speed of 630 r min^{-1} can produce nearly excellent surface integrity. Grain structure observations over the subsurface reveal three different layered zones including an ultrafine grain structure layer, a transitional grain structure layer and a substrate material layer. A significantly hardened (56% increase) surface layer on cutting-and-burnishing region comparing with the solely cutting region is detected. The subsurface grain features are induced by repeated thermo-mechanical functioning that causes grain refinement and thus materials hardening. The different surface integrities are the result of comprehensive functions of the machining parameters and combined drilling mechanism.

1. Introduction

In the development of manufacturing industries, the boring trepanning association (BTA) process came about chiefly as a by-product from World War II technology [1]. From that point, the technique is greatly applied in oil industries, engine crankshaft as well as die and mould manufacturing [2]. It is also broadly demanded in the field of aerospace industries and the rapidly developing high-speed trains. Herein, machining a long, uniform deep hole structure signifies great advances in the industrial manufacturing which facilitates industrial product upgrading and the development of new industries. Importantly, the finish surface quality of the deep hole directly affects the subsequent processing efficiency, precision, product lifetime and becomes a key factor in determining the usability of the product. Generally, BTA manufacturing is a sensitive operation task where the optimal coordination of the machining parameters and tool design for good output quality varies on different materials. In addition, it is a method that also depends on the skills and judgement of the operator during mechanical processing. Consequently, the finish quality can fluctuate among different machining batches. Meanwhile, a direct observation and measurement on the drilling procedure is extremely hard, due to the inclosed, long and narrow internal space created by the deep hole drilling. Due to the measurement limitations and the high costs of the studies, the relations between the finish quality (i.e. surface integrity of the inner machined surface) and machining parameters are poorly investigated in BTA deep hole drilling.

Surface integrity can be defined as topographical, mechanical,

* Corresponding author. School of Mechanical Engineering, North University of China, Taiyuan 030051, China.
** Corresponding author. School of Chemistry, Physics and Mechanical Engineering, Queensland University of Technology, 2 George street, Brisbane, QLD 4000, Australia.
E-mail addresses: shenxingquan@nuc.edu.cn (X. Shen), yuantong.gu@qut.edu.au (Y. Gu).
[1] H.Z. and A.B. contributed equally to this work.

http://dx.doi.org/10.1016/j.ijmachtools.2017.07.005
Received 13 April 2017; Received in revised form 20 July 2017; Accepted 21 July 2017
Available online 23 July 2017
0890-6955/

chemical and metallurgical characteristics of a manufactured surface and their relationship to the functional performance [3]. A clear connection can be found between the production process and the geometrical properties of the surface such as surface roughness, microgeometry as well as physical/mechanical property changes at the subsurface which include plastic deformation, phase transformations and microhardness [4–6]. Generally, the surface quality of a final product is considered a consequence of both the mechanical and thermal effects [7]. Under traditional machining process such as turning, milling and grinding, there forms various modified layers at the machined subsurfaces [8–11]. It is reported that a layer with increased hardness is observed on macroscale drilled nickel superalloy [12,13]. In BTA deep hole drilling, uniquely, intendedly designed guide pads come after the cutting edge and burnish the cut surface which deliberately generates a secondary processing step to the workpiece. During the above process, the hardened subsurface layers can increase pad wear and decrease machining quality. Akcan et al. [14] suggest that, without optimizing the parameters, the machined surface possesses high surface roughness (e.g. rifling marks) which brings difficulties to the subsequent finish processing. The BTA deep hole drilling under optimized parameters can produce high quality holes of high symmetry, accuracy in size, roundness, straightness and smooth finish surface. These rely on the special tool geometry and the settings of the drilling process where multiple machining effects take place in one continuous pass. During the process, rifling marks generated in BTA deep hole drilling (originated from self-excited vibration [15]) can cause unwanted surface roughness. Consequently, post-drilling measures aimed to perfect the surface quality become extremely difficult and time-consuming. Currently, comprehensive monitoring of the finish quality is hindered due to the large workpiece and the deep-hole bearing structure. It has been shown by Griffiths et al. [16,17] that the use of stylus gives incomplete assessment of the BTA machined surface (due to the limited travel distance) which also fails to reveal the existence of the folding induced material overhang. Apart from few studies on simulation based analysis of stability and vibration of deep hole machining [2,18,19], researches focusing on the BTA drilling, especially subsurface structure of the BTA processed surface are rare. Given the complex machining mechanism, it is also of great importance to observe and analyze the material subsurface properties generated by the BTA process.

Proper selection of machining parameters (e.g., tool geometry, feedrate and speed) is critical to BTA deep hole drilling whereas how these parameters would affect the surface integrity is largely unknown. Rao and Shunmugam [20] found that there is an optimum value for feed rate, beyond which point the microhardness value is barely affected. Contrary to the above findings, El-Khabeery et al. [21] report that microhardness continues to increase with increased feedrate. A great scatter in different measures of surface integrity has been observed, which makes it difficult to evaluate the guide pad performance for different process parameters.

Table 1
Drilling parameters used in this work.

Feed (mm min^{-1})	10,20, 28, 36
Speed (r min^{-1})	360, 452, 630, 800
Depth (mm)	100

Considering the incomplete evaluation on BTA deep hole drilling, it is necessary to systematically explore the internal surface integrity of the deep holes to provide guidance to the machining process. In this work, we have investigated the surface integrity of BTA processed cast iron workpieces which are widely used as automobile engine crankshafts, gear shafts and cylinders due to its high strength, excellent vibration absorption and wear-resistance [22,23]. By characterizing the surface/-subsurface integrity of the workpiece produced under various machining parameters, we are to retroactively derive the key mechanisms in BTA drilling process and develop dependent relationship between the processing quality and the machining parameters (i.e. drill speed and feedrate). In detail, the workpieces subjected to different processing parameters are dissected to allow surface roughness characterization of their inner surface. Subsequently, detailed surface morphologies are observed via scanning electron microscopy (SEM). The deformed subsurface grain structures are observed by SEM under backscatter electron (BSE) and electron backscattered diffraction (EBSD) imaging modes. The hardness values along the deformed subsurface is collected which shows a noticeable hardening effect caused by burnishing effect from the guide pad. The characterization results are compared and discussed with the machining parameters which provide valuable insights to the BTA deep hole drilling.

2. Experimental details

2.1. BTA deep hole drilling tests

The deep hole drilling processes are performed on a BTA machine with a rotating workpiece that is machined using a Sandvik BTA solid drilling tool (30 mm in diameter). The BTA drilling system is actually used in the high-speed train hollow-axle production process. The materials of the workpieces are cast iron having 80 mm in diameter and 1800 mm in length as shown in Fig. 1a. To investigate the surface integrity of the workpieces subjected to different drilling conditions, factorial runs were conducted using the parameters presented in Table 1.

2.2. Sample preparations

To obtain workpieces containing both cutting and burnishing regions respectively, the drilling process is stopped quickly as designed, which provides feasibility for recording the combined deep hole drilling

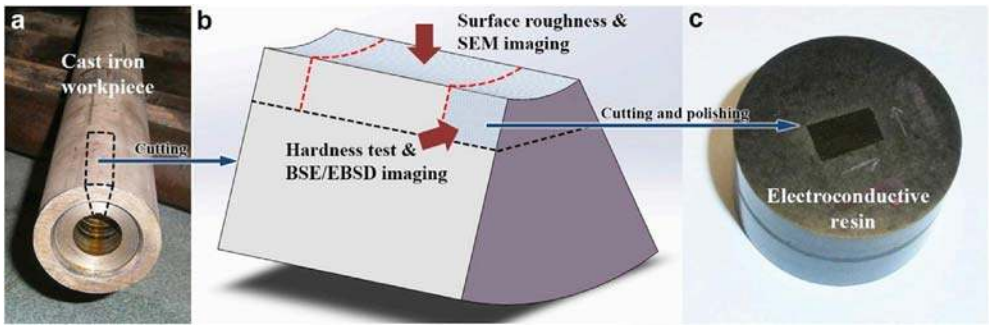

Fig. 1. (a) Photo of a BTA drilling machined workpiece from which individual pieces are dissected as marked by the dashed line. (b) Schematic illustration of a dissected workpiece on which different tests are performed as pointed. Roughness measurement and SEM secondary electron imaging tests are carried on the upper surface while hardness test and backscattered electron (BSE) as well as electron backscattered diffraction (EBSD) imaging are conducted on the side cross section. (c) Photo showing a sample prepared for the hardness, BSE and EBSD tests. The sample is embedded in electroconductive resin followed by polishing. The side cross section is facing up as indicated.

machining effect. After the BTA process, the samples are trimmed to obtain a blind hole which is longer than the length of the drilling depth. Then, the samples are dissected (shown as the area marked by the dash line in Fig. 1a) to facilitate close analysis of the machined surface and the subsurface. As depicted in Fig. 1b, wedge blocks are cut out from the sample, which contain a drilled surface and a cross sectional profile perpendicular to the drilled surface. Further analysis on the wedge block includes surface roughness measurement on the machined surface where morphological observations are also carried out using SEM. Roughness data is collected from 5 different locations for each sample. The mechanical properties of the subsurface are determined by conducting nanoindentation on the cross section along the longitudinal direction of the workpiece. The deformation behavior is closely observed at micrometer scale using BSD and EBSD imaging inside a SEM. To accommodate the hardness test and EBSD measurements, the dissected workpiece is further cut into a smaller piece (shown by the dash lines in Fig. 1b). The smaller workpiece is then embedded in electroconductive resin (Fig. 1c), having the surface polished for SEM imaging.

2.3. Measurements and characterizations

The surface finish qualities are measured using the Talysurf stylus at various positions. The values of the roughness parameters R_b, R_a, and R_zJIS for each sample are collected. All samples are examined on a Zeiss Sigma VP Field Emission SEM at 15 kV accelerating voltage over a wide range of magnifications. For metallographic examination, the drilled samples were prepared by hot mounting in an electroconductive resin to provide excellent imaging quality inside the SEM. All samples were polished using an automatic polishing machine, with an individual load of 20N, considering the sensitivity of the subsurface preparation. Thereafter, the specimens were cleaned using 2% Nital and then were dried. A completed SEM imaging sample is shown in Fig. 1c. BSE/EBSD techniques are adopted to assess the microstructure of the polished workpiece samples from different drilling conditions. All BSE/EBSD studies are carried out on a JEOL 7001F SEM at a working distance of 8.5 mm and accelerating voltage of 25 kV. Nanoindentation is used to determine the hardness profile on the deformation layers and is performed using Hysitron TI 950 TriboIndentor at a load of 8000 μN.

3. Results and discussion

3.1. BTA deep hole drilling mechanism

Unlike conventional processing techniques, BTA deep hole drilling involves a guiding system and a swarf removing system where the guiding pads (Fig. 2a) function as cutting force balancing, steering and polishing tool. A detailed illustration of the guiding pad incorporated BTA deep hole drilling system is presented in Fig. 2 having the main elements of drill head marked and named as listed in Fig. 2f. The staggered-edge drill head (as shown in Fig. 2b and d) with an asymmetric

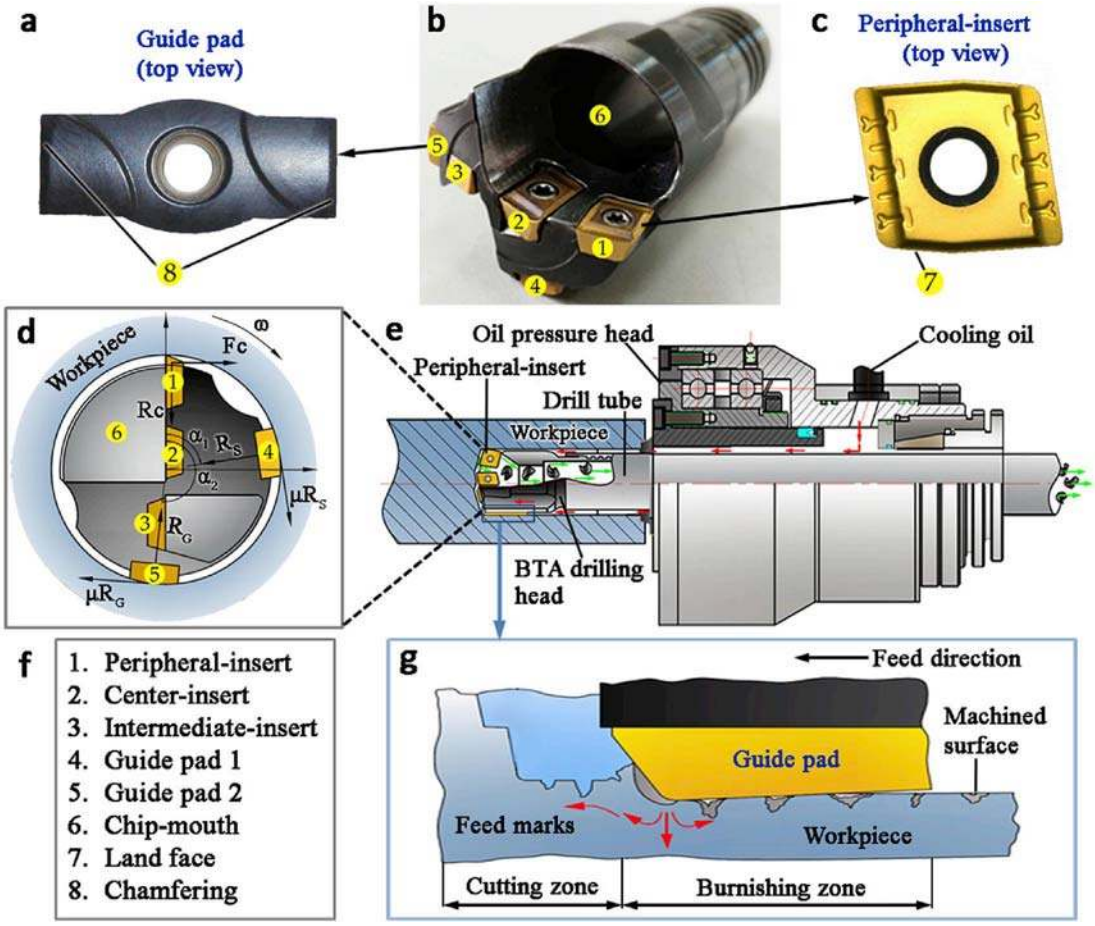

Fig. 2. (a) Photography showing a guide pad where it possesses chamfering as pointed and named in (f). (b) Image of a BTA deep hole drilling head where the individual parts are marked as listed in (f). (c) Image of a peripheral-insert enlarged from component No.1 from (b). (d) Schematic illustration of the BTA deep hole drilling head from a side view perspective enlarged from (e). (e) Schematic showing the entire BTA drilling system including drilling head, cooling oil, oil pressure head, peripheral-insert and drill tube as indicated. (f) List of names showing individual parts as marked by the yellow circles in figure a–d. (g) Schematic showing the cutting-burnishing combined machining mechanism of the BTA drilling process. (For interpretation of the references to colour in this figure legend, the reader is referred to the web version of this article.)

structure is called self-piloting tool [16,24], which features two guiding pads (indicated as Guide pad 1 and 2 by component No.4 and 5 in Fig. 2d) locating respectively at around 90° and 180° with respect to the inserts. There are three inserts (No. 1–3 shown in Fig. 2b and d) among which the peripheral-insert has a designed land face as shown in Fig. 2c. During machining with self-piloting tools, the two guiding pads, subjected to the cutting force (R_{G1} and R_{G2}) as well as the friction force (μR_{G1} and μR_{G2}), rub against the bore wall which induce a burnishing effect. Correspondingly, The construction of the drill head provides such drilling mechanism that maintains balance to the system and allows self-steering along the hole [16]. Meanwhile, a high pressure cutting fluid is introduced into the machining zone through the annular clearance between the drill tube and machined hole (indicated by the red arrows as inlet and green arrows as outlet direction, Fig. 2e). The cutting fluid carries away machining chips under a high speed through the tunnel of the drill tube avoiding contacts between the machined surface and the chips.

Based on the constructional characteristics of the drilling system, the machining itself performs a multi-processing task. As investigated by Griffiths [24] through step-wise recording the burnishing process on a quick-stop, the mechanism of BTA deep hole drilling is elaborated. Initially, rotation of the workpiece is accompanied by the engaging of the drilling head. Since the cutting edge interact with the workpiece prior to the guiding pads, it delivers a cutting and a burnishing zone as shown in the schematic diagram in Fig. 2g (actual presentation of the stair-stepping zones can also be found in Fig. 7b). In the cutting zone, a ridge of work material caused by the squashing of guide pads is shoved by the land face of peripheral-insert. In the burnishing zone, the extrusion force generates Hertzian contact stresses at the edge of cut surface when the stress exceeds the yield strength of the pristine material. As a result, the material deforms plastically at the surface where the surface ridges are compressed and flattened as the materials migrate into the valleys between the peaks (Fig. 2g). The surface layer of the bore is burnished as the guide pads mow over the machined surface. Overall, the BTA deep hole drilling can be considered as a cutting-burnishing combined machining, given the cutting and burnishing are supplementary to each other. It is clear that the guide pads with guiding and burnishing functions play a key role in deep hole drilling which also determine the size of the hole. This machining process continues along the entire workpiece, enabling the machining to produce smooth surface finish which is not obtainable with other finishing processes such as reaming, rolling and grinding [17].

3.2. Surface roughness

The relation between machining parameters and the roughness generated at the internal surface after BTA deep hole drilling is investigated. To describe the material roughness from multiple perspectives, different evaluation parameters are applied in this study. They include R_b R_a, and R_zJIS, where R_t represents the maximum peak-to-valley height of the roughness profile, R_a is arithmetic average of absolute value and R_zJIS is the 10 point average value of the five highest peaks and five lowest valleys. In Fig. 3, the bar charts reveal the variations of roughness R_b R_a, and R_zJIS under different feedrates and drilling speeds respectively. Firstly, R_t values are shown to be considerably larger than that of R_a and R_zJIS and shows nonlinear characteristics from both the feedrate and speed variation experiments. This nonlinearity indicates the unstable phenomenon of deep hole drilling having unexpected overcut or ineffective burnishing. The value of R_t can be significantly high, even the overall machining delivers smooth internal surface. This is caused by the abrupt forward sliding phenomenon of drill head which reflects the unstable essence of BTA deep hole drilling.

An improvement in the finish quality (i.e. decrease in R_a value) is observed in Fig. 3a as the feedrate increases from 10 mm min^{-1} to 28 mm min^{-1}. In the conventional machining, elevating the feedrate can lead to increase in the roughness [25,26]. In contrast, BTA Deep hole drilling is a drilling-burnishing combined process where the surface quality of the workpiece is also greatly determined by the burnishing action of guiding pads that comes after the cutting action. The increase in feedrate produces higher thrust which in return elevates the radial force on the guide pads. Hence, the strengthened burnishing effect leads to an improvement of the finish quality. However, the excessively high feedrate can result in heavy load burnishing effect which produces brittle surface flaking and generate insufficient burnishing. Discussions relating to the surface microstructure can be found in the following section (Fig. 5). Moreover, over increasing the feedrate can reduce stability of the drilling system. The above factors can contribute to the degrading finish quality (increase in roughness) as observed under higher feedrate (36 mm min^{-1}). It is worth noting that the excessive feedrate can lead to thicker chips (breaking and exclusion of the chips become challenging) and increases the risk of chip blocking which can be detrimental to the whole drilling system.

When the feedrate is fixed, an improvement in the finish quality is observed as the speed is increased from 360 r min^{-1} to 630 r min^{-1} (Fig. 3b). Increase in drill speed leads to an increment in the burnishing frequency. Besides, it leads to a decrease in the scale and material tearing. However, as the speed is increased to 800 r min^{-1}, a noticeable worsening of the finish quality is detected. This can be attributed to the increased plowing effects of the micro-chips and built-up edges. Meanwhile, an increased system vibration under excessive drilling speed takes place due to the weak stiffness nature of the cutting-boring bar system. It is notable that the combined feedrate and speed parameters in BTA drilling generate various finish quality and it is a trade-off when increasing either of these parameters. To produce optimal surface quality, a number of tests are conducted on the machined workpiece as shown

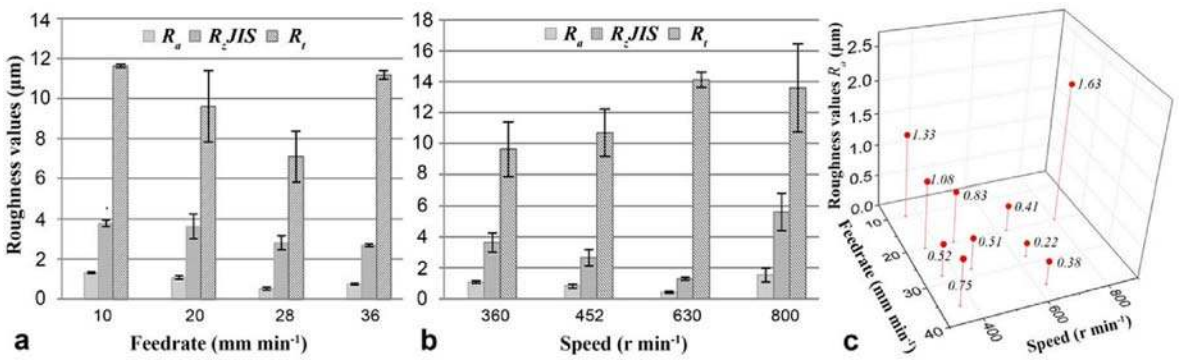

Fig. 3. (a) Bar chart showing the relation between the machining feedrate against the roughness values measured from the processed workpiece. The speed is fixed at 360 r min^{-1} in these measurements. (b) Bar chart showing the roughness values measured from samples processed with fixed feedrate (20 mm min^{-1}) and various speeds. The error bar is generated through solving the standard deviation of 5 measurement values. (c) 3D point scatter showing the roughness value plotted against changes in both speed and feedrate.

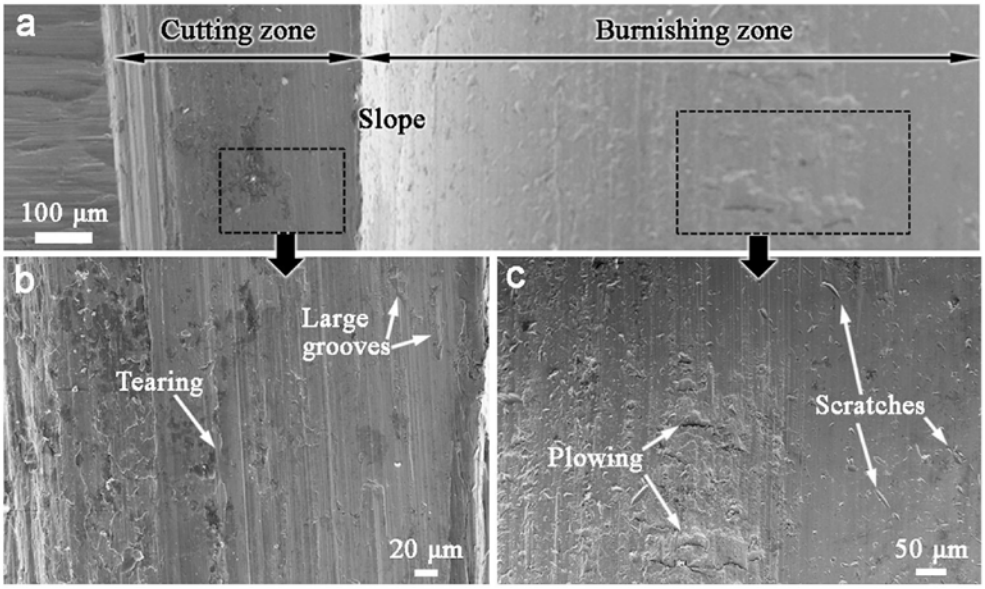

Fig. 4. (a) SEM image of the dissected cross section of workpiece where the cutting and burnishing zones are shown. Such a sample is obtained by stopping and retracting the drilling quickly in the course of drilling process. The drilling is conducted at a feedrate of 20 mm min^{-1} and a drill speed of 800 r min^{-1}. (b) SEM image depicting the microstructures from the cutting zone where material tearing and formation of large grooves can be seen. (c) SEM image of the enlarged burnishing zone where surface features such as excessive plowing and scratches are pointed by the arrows.

in Fig. 3c. It is found that when a moderate feedrate of 28 mm min^{-1} is combined with a comparatively high speed of 630 r min^{-1}, an optimal finish quality is obtained with a minimum level of roughness (R_a = 0.22 μm).

3.3. Microstructures at the machined surface

The surface characteristics of the machined workpieces are revealed by a SEM over a wide range of magnifications. Under SEM secondary electron imaging, the stair-stepping geometric structure characteristics show that the cutting zone has a height difference and distinctive features comparing with that from the burnishing zone, as show in Fig. 4a. It signifies a notable machining of the guide pads on the cut surface. Furthermore, a considerable variation in the appearances of the cut and burnished surface can be observed by enlarging the images from each area (marked by the black dash boxes in Fig. 4a). The enlarged cutting and burnishing zones are depicted in Fig. 4b and c respectively. In Fig. 4b, a coarse-scale surface scratch showing an irregular series of brittle material tearing-off from the surface layer, plateaus and large grooves. Under relatively high speed, the gradually blunted tip of the peripheral-insert and the built-up edge attached to the tip cause repeated burnishing to the workpiece that leads to material flaking. At the same time, the shaving effect of the blunted tip brings about material tearing and thus, irregular grooves as shown in Fig. 4b. Comparing with the microstructures in the cutting zone, an overall improvement in the finish quality is observed in the burnishing zone (Fig. 4c) where the guide pads flatten the wavy grooves after material cutting. The guide pad chamfering induces plowing phenomenon which gradually alleviates as the guide pads completely pass through the region. This is depicted in Fig. 4c where the right side of the surface has notably smoother surface than the left side. Nevertheless, scratches from the chips or built-up edges still exist in the burnishing zone (Fig. 4c), due to the interactions between the burnished surface and irregular built-up edges as well as chips welded to the guide pad. The geometric structure and surface characteristics contribute collectively to the deep hole drilling mechanism.

The variations in microstructures on the burnished surface with respect to different machining conditions are observed in detail. Uniformly oriented surface plateaus and grooves after cutting-burnishing effect can be observed in Fig. 5. The SEM images in Fig. 5a and b reveal a unique feature of BTA deep hole machining, where grooves and plateaus exist after they are modified by the guide pads. This is because the limited burnishing force results in insufficient burnishing under large

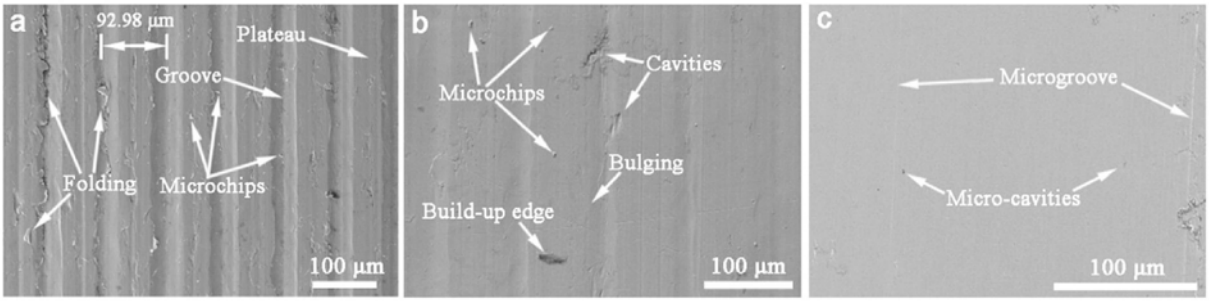

Fig. 5. SEM image showing the deep hole surfaces microstructure under different machining conditions (a) feedrate = 36 mm min^{-1}, Speed = 360r min^{-1}; (b) feedrate = 28 mm min^{-1}, Speed = 360r min^{-1}; (c) feedrate = 28 mm min^{-1}, Speed = 630r min^{-1}. (a) SEM image depicting the coarse surface damage where a series of grooves, plateaus, microchips and folding actions. The spacing between the plateaus and grooves are measured; (b) SEM image showing the surface microstructures with microchips, cavities and build-up edges. (c) SEM image revealing a smooth surface with few presence of microgroove and micro-cavities.

feedrate where the workpiece ridges cannot be fully spread to smoothen the surface roughness. Regardless, it is in a good agreement with the described surface forming mechanism in Section 3.1, that the guide pads have burnished the wave peak and shoved the materials with plastic flowing. When the guide pads mow over the peaks, they extrude the materials into the grooves such as the bulging produced at both sides of the plateau region.

When drilling at a low drilling speed and high feedrate (Fig. 5a), it can be seen that the flat plateaus and grooves appear to be approximately uniformly spaced, where the spacing (as the measurement shown in Fig. 5a) between the neighboring grooves being slightly smaller than the feedrate value (0.1 mm rev^{-1}). The reduced feed spacing proves the presence of the secondary ridges and grooves. In this case, when the land face works in conjunction with the blunted guide-pad chamfering, they grind the grooves and plateaus where the combination functions as a ponderous extrusion process instead of sharp cutting. The fragments on the plateaus could not be thoroughly truncated under the incomplete extrusion. Concurrently, the fragments are upwarped by the grinding guide pads or removed by the land face. Broken fragments are shown as debris found lodging on top of the plateaus. When the squashed thin-materials are further extruded, material folding can be observed in the burnished regions (edges and peak of the plateaus) [17]. Part of the plateau materials is broken away to produce microchips. Under certain occasions, the microchips can be swept away from the substrate and burnished again by the guide pads. Then, they are smeared into the surface to form scales on the machined surface.

With the feedrate decreased from 36 mm min^{-1} to 28 mm min^{-1} under the speed of 360 r min^{-1} (Fig. 5b), the insufficient burnishing can be effectively alleviated. Therefore, the coarse surface damage is weakened. It is notable that the microstructure characteristics in Fig. 5a and b are consistent with the roughness values as previous shown in Fig. 3a. Nevertheless, they both show several microchips, large cavities and presence of built-up edge. In the meantime, the plateau bulging is more pronounced (wider plateau) in Fig. 5b that gives a clear indication of leveling the plateaus and valleys comparing with that in Fig. 5a. The cavities in Fig. 5b are considered as a result of nonuniform spreading of the materials. When the drill speed is increased to 630 $rmin^{-1}$ (i.e. increase in the burnishing frequency) while maintaining the same feedrate as in Fig. 5b, a further decreased in surface roughness is observed in Fig. 5c. As depicted, the plateaus and grooves become nearly undetectable having the extremely smooth surface with outstanding burnishing. Nevertheless, micro-scale surface damage still exists such as long straight microgrooves and micro-cavities. To some extent, this is resulted from the unstable drilling and inhomogeneous burnishing. Despite the microgrooves and occasional cavities, the overall surface integrity is considered ideal.

3.4. Microstructure at the machined subsurface

To investigate the properties of the machined subsurface, a metallurgy analysis of the grain structure is carried out. BSE/EBSD imaging techniques reveal specific and overall grain structures of the workpiece material at the burnished zone as shown in Fig. 6. A magnified observation on the edge of the cross-section (Fig. 6a) reveals the subsurface grain structure from the machined sample (drilling speed of 630 r min^{-1} and feedrate of 20 mm min^{-1}) that shows extremely small crystalline grains structures. Based on the structural characteristics, the observed outer layer is named ultrafine grain structure (UGS) layer. Following the UGS layer (Fig. 6a left side), a layer of larger grains (maximum grain size around 2μm) is observed which is named as transitional grain structure (TGS). The grains from TGS layer are significantly smaller than that from the substrate material (SM) which possesses grains with diameter sizes between 20 and 40 μm. A similar subsurface layer is observed after micro drilling processes [12,13,27].

The microstructure layer of UGS can be correlated to the so-called hardened “white layer” as observed under optical microscope in conventional machining [3,9]. Layer TGS exhibits a transitional grain structure which gradually merge into the substrate material (layer SM). The ultra-fine, narrow and long bands of grains in the UGS layer could be a result of violent grain deformation from machining induced lattice rotation in surface-modified layers [13]. Furthermore, the thickness of UGS and TGS layer are slightly uneven which can be attributed to the nonlinear burnishing effect. Under a low magnification with BSD (Fig. 6c) and the corresponding EBSD imaging (Fig. 6d) with an inverse pole figure (IPF) color map, it depicts grains with different orientations. The sub-grain boundaries and the associated gradients in the IPF color map show well-defined grain distributions from the substrate region and the deformed layers. It can be seen that the combined thickness of the deformation layers (UGS and TGS) is relatively narrow (around 100 μm) due to the low resultant force caused by the intrinsic insert distribution

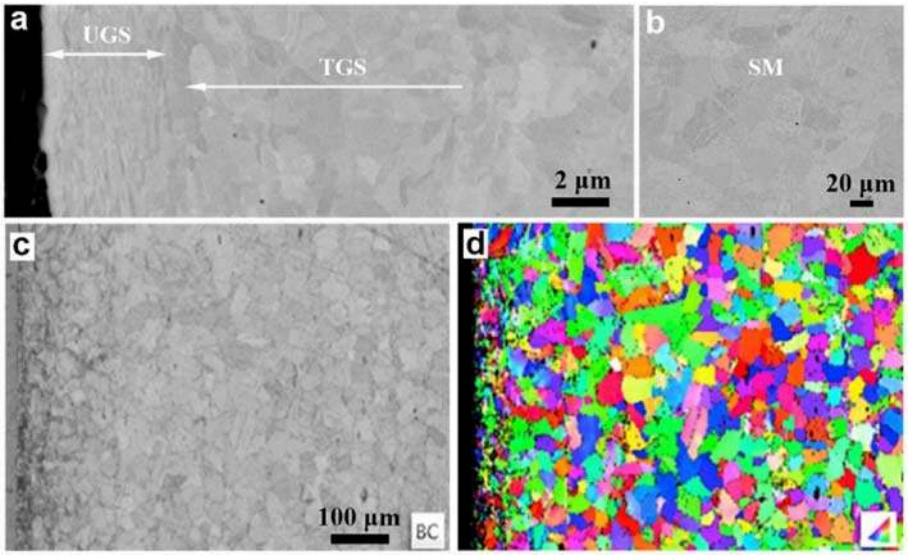

Fig. 6. (a) BSE image showing the micro-sale grain structure from the subsurface layers of a workpiece (speed 630 r min^{-1} with a feedrate of 20 mm min^{-1}) (b) SEM BSE imaging showing the grain structure taken from the substrate material. (c) SEM BSE image and the corresponding EBSD image (d) taken under low magnifications where a grain size gradient can be seen from the machined surface to the substrate material.

feature (intermediate insert locates at around 180° with regard to the other two inserts) which balance the forces in the multi-insert drill. It is clear that the deformation range along the substrate materials is not significant in BTA deep hole drilling.

3.5. Nano-hardness profile

To investigate the mechanical properties of the deformation layers, nano-hardness measurements are carried out which cover all three layers from both the cutting and burnishing zones respectively. The nano-indentation tests are implemented at the cross-profile of the subsurface layer leaving obvious indent marks as shown in Fig. 7a and c. The stair-stepping sample configuration is depicted in Fig. 7b from which the regions for hardness tests are selected. It can be seen from Fig. 7c (tests from the burnishing zone) that the indent marks closer to the surface are considerably smaller than the ones locating at the substrate side. The smaller indent mark indicates a higher hardness value. The one-to-one correspondence between the indent marks and hardness values from the cutting and burnishing zones are indicated by the red and blue dash arrows respectively (Fig. 7d). In comparison, indent marks from the cutting zone (Fig. 7a) are mostly uniform in shape. It is evident from the two curves in Fig. 7d that the UGS layer in the burnishing zone maintains appreciably higher values of nanohardness compared with that at cutting zone with an increment of 56%. Moving away from the machined surface, the hardness decreases sharply as the depth increases until it reaches the hardness of the substrate material (around 2.8 GPa). The gradient variation in hardness can be attributed to the ultrafine grain structures evidenced by the BSE observation in Fig. 6a.

The hardness and yield stress of the material typically increase with decreasing grain size [28], which is in good accordance with the Hall-Petch effect [29,30]. On the other hand, the large grains provide additional space for the movement of dislocations before they are pinned at grain boundaries [31]. The liberation of dislocation movement means less internal stress between the grains, and vice versa. Smaller grains lead to a higher total grain boundary density. The grain boundaries can act as a barrier to dislocation motion [32]. Consequently, this causes more dislocation blocks, higher dislocation densities and increased hardness from the higher required deformation energy [13]. It is believed that the combination of the cutting-burnishing actions and the BTA drill head geometry produce grain deformation which is different from other machining. As previously described, the burnishing effect of guide pads has generated a secondary deformation on the machined surface with higher degree of plastic deformation accompanied by heat effect. Combining with the continuous cyclic plastic deformation, higher strain hardening on the surface layer takes place due to the rapid cyclic thermo-mechanical mechanism. The resulting effect produces smaller grain sizes. The existence of the hardened surface is also caused by the sufficient cooling oil supply, which leads to quench hardening of the surface layer [24].

Further investigation of the impacts of feedrate and drilling speed on the average hardness in UGS layer is summarized in Fig. 8a and b respectively. The feedrate-hardness relation shows a turning curvature where the minimum hardness value can be found at an intermediate feedrate of 28 mm min^{-1} (Fig. 8a). Under this feedrate, it generates a better surface quality as previously shown. This is because of the burnishing effect from the two guide pads that possess a certain length. Under a constant speed, lower feedrate indicates more frequent machining effect by the guide pads on a unit sample surface area. Concurrently, thermal energy from cutting also increases with the increasing feedrate [33], and the temperature generated during deep hole drilling can exceed 500 °C [24,34]. The grain boundary separation is generated under cyclic mechanical loading and thermal effect, which is bound to produce premature failure of specimens. Meanwhile, the partial decomposition of the matrix produces a softer ferrite as a result of thermal cycling between 120 and 500 °C [31] and leads to material softening. High ferrite content in the specimen leads to lower cutting force which also contributes to the low hardness [35]. The above complex effect can ultimately reduce the hardness. The decreasing hardness

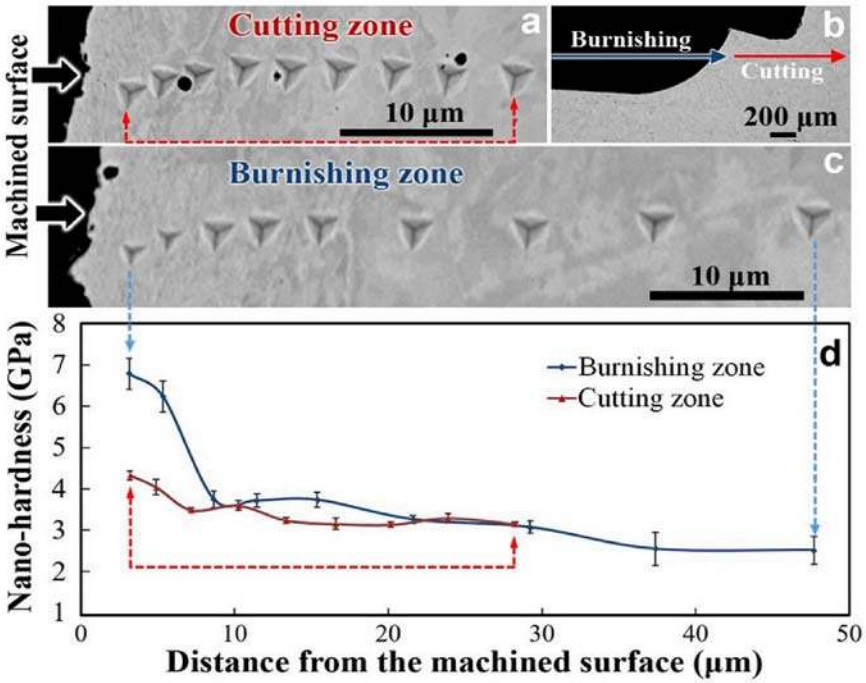

Fig. 7. (a) SEM image showing the marks put by nanoindentation near the surface from the cutting zone which is also indicated in figure (b). (b) Side-view, low magnification SEM image of the workpiece containing both cutting and burnishing zone where nanoindentation tests are performed. (c) SEM image showing the indentation at different layers from the burnishing zone. (d) Plot presenting the subsurface nano-hardness values from both the cutting (red points) and burnishing (blue points) zones. Each point can be aligned one-to-one with the indent point from figure (a) and (c) as marked by the red and blue arrows. (For interpretation of the references to colour in this figure legend, the reader is referred to the web version of this article.)

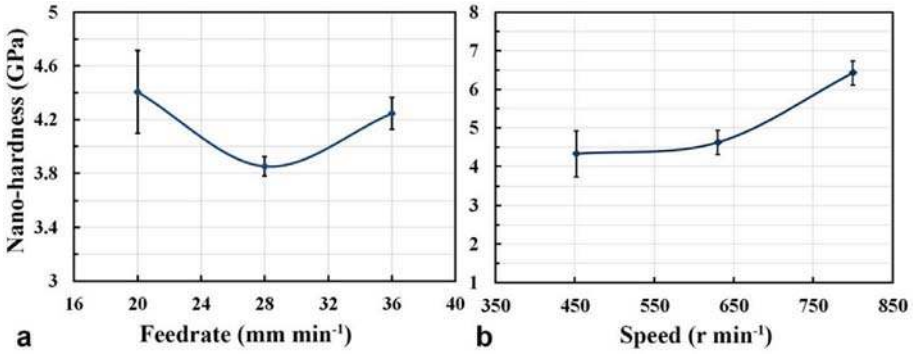

Fig. 8. (a) Plot showing the average nanohardness of UGS layer measured from various feedrate under the constant speed of 630 r min^{-1}. (b) Plot showing the average nanohardness of UGS layer taken from different speed parameters under the constant feedrate of 36 mm min^{-1}.

characteristic with the feedrate increase reveals benefits of excellent cutting property and low tool-wear [36,37]. As the feedrate continuously increases, thermal softening effect may not be consistently significant due to the instant exposure of workpiece under high temperature. Besides, the abundant supply of cooling liquid immediately quenches the surface layer [20] and work hardening strengthens the burnishing effect. In comparison, changes in hardness with regards to drilling speed elevation are noticeably larger. Under the constant feedrate, increase in the drilling speed directly leads to enhanced burnishing frequencies, as well as thermo-mechanical effects. Consequently, the hardness value increases continuously from 452 r min^{-1} to 800 r min^{-1}. Given the delicate impact to the nano-hardness, it is considered that the BTA drilling process is more sensitive to the changes in feedrate.

4. Conclusions

In summary, the surface integrity and deformation features in BTA deep hole drilling are investigated by measuring workpieces produced under various machining parameter combinations. From the above study, the following main conclusions can be drawn.

(1) Investigating the macro and micro surface deformation behavior of the machined cast iron workpiece, accompanied by the drilling tool geometry analysis, it confirms a burnishing effect from the guide pads which function as a secondary machining that comes after the cutting from the inserts. The interdependent relation between the cutting and burnishing effects is exclusive to BTA deep hole drilling and such unique feature can result in machined topological features such as plateaus, grooves, folding and cavities of different sizes. These surface features can be alleviated by changing the machining parameters.

(2) There is an optimum combination of feedrate (28 mm min^{-1}) and speed (630 r min^{-1}) for machining cast iron workpiece where BTA deep hole drilling produces an excellent surface integrity. Such a smooth machined surface comes from the interdepending cutting-burnishing process. In general, higher feedrate promotes burnishing effect while excessively high feedrate causes incomplete burnishing in the drilling system. Speed increase can enhance burnishing frequency which produces better surface quality while an excessive speed can result in the over-plowing effect and causes system vibration with the system being intrinsically weak in stiffness and the structure being relatively instable.

(3) Beneath the machined surface, metallographic analysis reveals distinctive deformation layers with different grain sizes. Under the burnished surface, there forms an UGS layer with significantly higher hardness (6.8 GPa) which is around 56% higher than that from the cutting zone and around 140% higher than the hardness value of the substrate materials. Formation of the different grain size distribution at the machined subsurface is caused by the cutting-burnishing effect and is responsible for the hardness difference. Smaller grains lead to a higher total grain boundary density and more dislocation blocks, and thus higher hardness at the UGS layer.

(4) Nanohardness value from different machining parameters shows that large feedrate and speed increase the work hardening due to the strengthening of burnishing effect. As the cutting heat builds up under low feedrate machining, it causes partial decomposition of the matrix into softer ferrite which may contribute to the lower hardness. Nevertheless, the role of thermal impact needs to be further analyzed when precise measurement of the working environment temperature can be achieved.

In all, machining parameters in the cutting-burnishing combined BTA deep hole drilling is crucial to the surface integrity of the product. From this point on, the perfected surface integrity can greatly facilitate application of the machined product and improve product quality.

Acknowledgments

The author would like to thank technical supports from the Central Analytical Research Facility (CARF) of Queensland University of Technology (QUT). Acknowledgement also goes to funding support from the Australian Research Council (ARC) Discovery Project [DP170102861], International S&T Cooperation Program of China [2013DFA70770] and the State Scholarship Fund from the China Scholarship Council (CSC).

References

[1] H.J. Swinehart, Gun drilling, trepanning, and deep hole machining, American Society of Tool and Manufacturing Engineers, Dearborn, Michigan, 1967 p vi-2.
[2] J.-H. Chin, C.-T. Hsieh, L.-W. Lee, The shaft behavior of BTA deep hole drilling tool, Int. J. Mech. Sci. 38 (1996) 461–482.
[3] B. Griffiths, Manufacturing Surface Technology: Surface Integrity and Functional Performance, Elsevier, 2001.
[4] J. Kwong, D. Axinte, P. Withers, M. Hardy, Minor cutting edge–workpiece interactions in drilling of an advanced nickel-based superalloy, Int. J. Mach. Tools Manuf. 49 (2009) 645–658.
[5] M. Field, J.F. Kahles, Review of surface integrity of machined components, Ann. CIRP 20 (1971) 153–163.
[6] R. M'Saoubi, J. Outeiro, H. Chandrasekaran, O. Dillon Jr., I. Jawahir, A review of surface integrity in machining and its impact on functional performance and life of machined products, Int. J. Sustain. Manuf. 1 (2008) 203–236.
[7] J. Kwong, D. Axinte, P. Withers, The sensitivity of Ni-based superalloy to hole making operations: influence of process parameters on subsurface damage and residual stress, J. Mater. Process. Technol. 209 (2009) 3968–3977.
[8] S. Bosheh, P. Mativenga, White layer formation in hard turning of H13 tool steel at high cutting speeds using CBN tooling, Int. J. Mach. Tools Manuf. 46 (2006) 225–233.
[9] B. Griffiths, Mechanisms of white layer generation with reference to machining and deformation processes, J. Tribol. ASME) 109 (1987) 525–530.

[10] J. Sun, Y. Guo, A comprehensive experimental study on surface integrity by end milling Ti–6Al–4V, J. Mater. Process. Technol. 209 (2009) 4036–4042.
[11] W. Li, N. Tao, K. Lu, Fabrication of a gradient nano-micro-structured surface layer on bulk copper by means of a surface mechanical grinding treatment, Scr. Mater. 59 (2008) 546–549.
[12] A. Sharman, A. Amarasinghe, K. Ridgway, Tool life and surface integrity aspects when drilling and hole making in Inconel 718, J. Mater. Process. Technol. 200 (2008) 424–432.
[13] M. Imran, P.T. Mativenga, A. Gholinia, P.J. Withers, Evaluation of surface integrity in micro drilling process for nickel-based superalloy, Int. J. Adv. Manuf. Technol. 55 (2011) 465–476.
[14] S. Akcan, W.S. Shah, S. Moylan, S. Chandrasekar, P. Chhabra, H. Yang, Formation of white layers in steels by machining and their characteristics, Metall. Mater. Trans. A 33 (2002) 1245–1254.
[15] K. Matsuzaki, T. Ryu, A. Sueoka, K. Tsukamoto, Theoretical and experimental study on rifling mark generating phenomena in BTA deep hole drilling process (generating mechanism and countermeasure), Int. J. Mach. Tools Manuf. 88 (2015) 194–205.
[16] B. Griffiths, in: An Investigation into the Role of the Burnishing Pads in the Deep Hole Drilling Process, Brunel University, 1982.
[17] B. Griffiths, Problems in measuring the topography of machined surfaces produced by plastic deformation mechanisms, Wear 109 (1986) 195–205.
[18] K. Lingfei, L. Yan, Z. Zhiyuan, Numerical investigating nonlinear dynamic responses to rotating deep-hole drilling shaft with multi-span intermediate supports, Int. J. Non-Linear Mech. 55 (2013) 170–179.
[19] H.M. Al-Wedyan, R.B. Bhat, K. Demirli, Whirling vibrations in boring trepanning association deep hole boring process: analytical and experimental investigations, J. Manuf. Sci. Eng. 129 (2007) 48–62.
[20] P.R. Rao, M. Shunmugam, Investigations into surface topography, microhardness and residual stress in boring trepanning association machining, Wear 119 (1987) 89–100.
[21] M. El-Khabeery, S. Saleh, M. Ramadan, Some observations of surface integrity of deep drilling holes, Wear 142 (1991) 331–349.
[22] D. Zeng, L. Lu, N. Zhang, Y. Zhang, J. Zhang, Investigation on the scuffing resistance of ductile cast iron as affected by fine particle bombardment to produce surface hardened layer and micro-dimpled surface, Wear 378 (2017) 174–182.
[23] H. Jang, K. Ko, S. Kim, R. Basch, J. Fash, The effect of metal fibers on the friction performance of automotive brake friction materials, Wear 256 (2004) 406–414.
[24] B. Griffiths, R. Grieve, The role of the burnishing pads in the mechanics of the deep drilling process, Int. J. Prod. Res. 23 (1985) 647–655.
[25] T. Özel, T.-K. Hsu, E. Zeren, Effects of cutting edge geometry, workpiece hardness, feed rate and cutting speed on surface roughness and forces in finish turning of hardened AISI H13 steel, Int. J. Adv. Manuf. Technol. 25 (2005) 262–269.
[26] D.K. Baek, T.J. Ko, H.S. Kim, Optimization of feedrate in a face milling operation using a surface roughness model, Int. J. Mach. Tools Manuf. 41 (2001) 451–462.
[27] D. Axinte, P. Andrews, Some considerations on tool wear and workpiece surface quality of holes finished by reaming or milling in a nickel base superalloy, Proc. Inst. Mech. Eng. Part B J. Eng. Manuf. 221 (2007) 591–603.
[28] J. Schiøtz, F.D. Di Tolla, K.W. Jacobsen, Softening of nanocrystalline metals at very small grain sizes, Nature 391 (1998) 561–563.
[29] N. Hansen, Hall–Petch relation and boundary strengthening, Scr. Mater. 51 (2004) 801–806.
[30] E. Hall, The deformation and ageing of mild steel: III discussion of results, Proc. Phys. Soc. Sect. B 64 (1951) 747–753.
[31] S. Buni, N. Raman, S. Seshan, The role of graphite morphology and matrix structure on low frequency thermal cycling of cast irons, Sadhana 29 (2004) 117–127.
[32] T. Britton, D. Randman, A. Wilkinson, Nanoindentation study of slip transfer phenomenon at grain boundaries, J. Mater. Res. 24 (2009) 607–615.
[33] R. Komanduri, Z. Hou, A review of the experimental techniques for the measurement of heat and temperatures generated in some manufacturing processes and tribology, Tribol. Int. 34 (2001) 653–682.
[34] H. Fuss, Aspekte zur Beeinflussung der Qualität von BTA-Tiefbohrungen[M], 1986 na.
[35] U. Şeker, H. Hasirci, Evaluation of machinability of austempered ductile irons in terms of cutting forces and surface quality, J. Mater. Process. Technol. 173 (2006) 260–268.
[36] M. Fattouh, M. El-Axir, S. Serage, Investigations into the burnishing of external cylindrical surfaces of 7030 Cu-Zn alloy, Wear 127 (1988) 123–137.
[37] H. Sasahara, The effect on fatigue life of residual stress and surface hardness resulting from different cutting conditions of 0.45% C steel, Int. J. Mach. Tools Manuf. 45 (2005) 131–136.